Optical properties of Pr and Eu-doped $SrAl_{12}O_{19}$: a theoretical study

Marcos V dos S Rezende[a], Jomar B Amaral[b], Mário EG Valerio[c], Robert A Jackson[d, *]

[a] Departamento de Física, Universidade Federal de Sergipe, 49500-000, Itabaiana - SE, Brazil
[b] Faculdade Estácio de Sergipe, 49020-530, Aracaju-SE, Brazil

[c] Departamento de Física, Universidade Federal de Sergipe, 49100-000, São Cristóvão - SE, Brazil
[d] School of Physical & Geographical Sciences, Keele University, Keele, Staffordshire, ST5 5BG, UK

Abstract: This paper describes a computational study of extrinsic defect and optical properties of $SrAl_{12}O_{19}$ induced by trivalent rare earth dopants. Solution energies for a range of possible doping mechanisms are calculated, and predictions made of doping sites and charge-compensation schemes. Atomistic modelling is used to calculate the symmetry and detailed geometry of the dopant ion-host lattice system, and this information is then used to calculate the crystal field parameters. It is found that the preferred doping mechanism for Pr is a substitution at Sr^{2+} sites, with charge compensation by anti-site and for Eu is a substitution at the Al^{3+} site. Crystal field parameters have been calculated and the results discussed in terms of optical properties of the doped systems. B^k_q values indicate that the site symmetry is D_{2h}. The transition levels are then calculated for the Pr^{3+} and Eu^{3+}-substituted material, and comparisons made with experimental results have a good agreement.

Keywords: optical properties, defects, europium, praseodymium

1. Introduction

In recent years, optical properties in rare earth-activated aluminate phosphors have been extensively investigated for many potential applications. For example, such as lamps, colour displays radiation dosimetry and X-ray imaging. The Strontium aluminates represent one of the classes of materials that may exhibit long lasting phosphorescence and luminescence when doped with trivalent rare-earth ions. Different crystalline compounds exist in the $SrO\text{-}Al_2O_3$ system and have been used as hosts for optical device materials, e.g. $SrAl_2O_4:Eu^{2+},Dy^{3+},B^{3+}$[1], $Sr_4Al_{14}O_{25}:Eu^{2+},Dy^{3+},B^{3+}$[2], $SrAl_4O_7:Eu^{2+},Dy^{3+}$[3], $Sr_2Al_6O_{11}: Eu^{2+}$[4].

In particular, $SrAl_{12}O_{19}$ phosphors have interesting optical properties when doped by rare-earth and transition metal ions. $SrAl_{12}O_{19}$:Mn is a green-emitting phosphor for plasma display panels [5]. $SrAl_{12}O_{19}:Pr^{3+}$ shows good laser properties [6].

$SrAl_{12}O_{19}:Eu^{2+},Dy^{3+}$ [7] are reported to exhibit high brightness and long-lasting phosphorescence.

$SrAl_{12}O_{19}$ is observed in hexagonal form [8] with the $P6_3$ space group. There is one strontium site and large coordination number (12) and large distances to nearest-neighbour oxygen ions (2.750–2.785 Å). There are five different aluminium sites. For the other strontium aluminates different crystallographic forms are observed depending on the $SrO:Al_2O_3$ ratio.

In the present paper a hybrid computer modelling method was employed, based on a combination of crystal field calculations, and energy minimisation. The method uses energy minimisation to predict the location of the dopant ion, and the relaxed positions of the surrounding ions. This information is then input into a crystal field calculation which obtains the crystal field parameters, B^k_q, which are then used to calculate the energies of the electronic transitions of Pr and Eu ions, which are then compared with recent experimental results.

2. Methodology

In this paper a hybrid modelling method was employed based on a combination of three different and complementary techniques: defect calculations based on energy minimisation, crystal field calculation via the simple overlap model and transition energy calculations.

For the first one, the methodology uses lattice energy minimisation, where the interactions between the ions present in the material are parameterised via interatomic Buckingham potentials supplemented by electrostatic interaction terms. The three constants involved in the Buckingham potentials for each pair of ions were obtained using empirical fitting methods embodied in the GULP code [9]. $SrAl_{12}O_{19}$ was modelled using the potential derived by Rezende et al. [10], and the structure determined by Lindop et al. [8]. The potentials for the trivalent rare earth ion–oxygen interactions were obtained from Araujo et al. [11]. Calculations of rare earth doping were performed using the Mott–Littleton method [12] in which atoms in a spherical region immediately surrounding the defect are treated explicitly, and a continuum approach is used for more distant regions of the lattice.

In the second step, the relaxed positions of the dopant and the surrounding ions are then input into a crystal field calculation which obtains the crystal field parameters, B^k_q, using the simple overlap model (SOM) [13].

In the third step, the B^k_q's were used to calculate the energies of the electronic transitions via the modified crystal field theory based on the Judd-Ofelt theory [14,15]. In this theory, the interaction between the rare-earth ion and the surrounding (host crystal) ions is given by crystal field Hamiltonian H_{CF}:

$$H_{CF} = \sum_{k,q} B_q^k C_q^k \tag{1}$$

where the C^k_q terms are the Racah spherical tensors and the B^k_q terms are the crystal field parameters. The electronic structure of the dopant ions were evaluated using the following Hamiltonian [16–18]:

$$H = H_{\text{free ion}} + H_{\text{CF}} = \sum_{i=0,2,4,6} F^i f_i + \zeta_{4f} A_{SO} + \alpha L(L+1) + \beta G(G_2) + \gamma G(R_7) + \sum_{i=2,3,4,6,7,8} T^i t_i + \sum_{i=0,2,4} M^i m_i + \sum_{i=2,4,6} P^i p_i + H_{CF} \tag{2}$$

All first terms are free ion parameters (ζ, α, β, γ, T^i, M^i and P^i) and were taken from [19]. The last term H_{CF} is the crystal field Hamiltonian given by (1). The energy levels were then computed within this framework, using the SPECTRA code [20].

3. Results and discussion

Doping of europium and praseodymium into $SrAl_{12}O_{19}$ has been considered. In either case there is the possibility that the dopant ion can substitute at either the Al^{3+} or the Sr^{2+} site. For substitution at the Al^{3+} site, no charge compensation is needed, and the solution process was assumed to be (where M is a rare earth ion):

$$0.5M_2O_3 + Al_{Al} \rightarrow M_{Al} + 0.5Al_2O_3 \tag{3}$$

It should be noticed that there are five non-equivalent Al^{3+} ions in the $SrAl_{12}O_{19}$ structure, labelled here as Al1, Al2, Al3, Al4 and Al5. So, there are five Al sites where the dopant could be located.

For substitution at the Sr^{2+} site, more than one possible mode of charge compensation mechanisms is possible. The charge compensation can occur by anti-site, strontium vacancies, oxygen interstitials or aluminium vacancies. The solution process was assumed to be, respectively:

$$0.5M_2O_3 + Sr_{Sr} + Al_{Al} \rightarrow \left(M^{\bullet}_{Sr} + Sr'_{Al}\right) + 0.5Al_2O_3 \tag{4}$$

$$M_2O_3 + 3Sr_{Sr} \rightarrow \left(2M^{\bullet}_{Sr} - V''_{Sr}\right) + 3SrO \tag{5}$$

$$M_2O_3 + 2Sr_{Sr} \rightarrow \left(2M^{\bullet}_{Sr} - O''_i\right) + 2SrO \tag{6}$$

$$1.5M_2O_3 + 3Sr_{Sr} + Al_{Al} \rightarrow \left(3M^{\bullet}_{Sr} - V'''_{Al}\right) + 3SrO + 0.5Al_2O_3 \quad (7)$$

It should be noticed that there is one non-equivalent Sr^{2+} ion in the $SrAl_{12}O_{19}$ structure. Nevertheless, the doping mechanism involving charge compensating defects will have more than one non-equivalent way of arranging the basic defects in the lattice, giving rise to different configurations of the full defect. Table 1 displays the Sr^{2+} ions position and notation used in mechanism involving charge compensating defects. Defects involving Sr^{2+} ions thus have to be modelled taking these six possible site, labelled here as $Sr^{(i)}$, $Sr^{(ii)}$, $Sr^{(iii)}$, $Sr^{(iv)}$, $Sr^{(v)}$ and $Sr^{(iv)}$ (showed in the Figure 1). One possible configuration, for example, is arranging two rare earth dopants in the $Sr^{(i)}$ and $Sr^{(ii)}$, sites accompanied by one $Sr^{(iii)}$ vacancy as charge compensation. The other defects just follow the same general idea.

In calculating the energetics of doping by rare earth ions, the defect formation energy is first calculated (see table 2). Then, the solution energy is calculated, which includes all the terms in the thermodynamic cycle involved when the solution process occurs, according to the following equation (substitution at the Al^{3+} site):

$$E_{Solution} = E_D + 0.5E_{Al_2O_3} - 0.5E_{M_2O_3} \quad (7)$$

$E_{Al_2O_3}$, E_{SrO} and $E_{M_2O_3}$ terms are lattice energies, E_D terms are defect formation energies, and Kroger–Vink notation [21] is employed for the defect formation energies. The interstitial site used is (1/3, 1/6, 1/8) that was easily found by simple inspection. This is possible due to the high symmetry in the lattice.

The formation energies reported in table 2 were calculated for a configuration consisting of the dopant and charge-compensating defects in neighbouring positions, meaning that the energies include the contribution of the binding energy of the defect. From table 3 it can be seen that for doping mechanism, involving Eu^{3+} and Pr^{3+} there is different behaviour. The Pr^{3+} ion is preferred to be incorporated at Sr^{2+} sites, with charge compensation by anti-site at 0 K, and at 293 K. Based in the lower energy value, the most likely mechanism involves a Pr ion in one Sr site plus a Sr at an Al^{3+} site. The other hand, the Eu^{3+} ion is preferred to be incorporated at the Al^{3+} site, at 0 K, and at 293 K.

The next stage involves calculation of the crystal field parameters B^k_q. These parameters are obtained using the non-relaxed lattice and relaxed positions of the nearest-neighbour ions to the rare earth dopant. The main difference between the two sets of B^k_q values is that in the non-relaxed lattice case the dopant ion is substituted at the host site without any relaxation of either the dopant ion or the surrounding ligand ions. For the relaxed lattice values, the ligand-dopant ion distances and positions are

obtained from the output of the defect calculation more provable obtained from atomistic simulation described above.

In table 3, the values of B^k_q parameters for the Pr^{3+} and Eu^{3+} ions are quoted for both the non-relaxed lattice and relaxed cases and the values are compared with those from reference [22]. It is worth stressing that the calculated values are true predictions using the B^k_q values obtained for the relaxed lattice surrounding the dopant, without any necessary previous knowledge of the spectra of the real system. The difference in B^k_q values between non-relaxed and relaxed systems show that the influence of relaxation in the neighbourhood of the dopant is important and should to be considered in the energy levels prediction.

Also in Table 3, it is clear that the values of calculated B^k_q's in this study and those presented in [22] are quite different. That occurs because of the way of the phenomenological measurements are performed in [22]. While in this paper we set out only the final positions of dopants and his first neighbors, Zandi *et al*. [22] part from the prior knowledge of the energy levels, a different theory of calculation is used and there is a co-doping with Mg^{2+}, which makes for example the final symmetry around the dopant to be calculated as D_{3h} and D_{2h} [23] in this work. The B^k_q's values can be better judged by using them to calculate transition energies, as has been done using the procedure described in methodology.

The B^2_0 parameter provides an indication of the strength of the electric dipole mechanism, and if $B^2_0=0$, no transitions allowed by the electric dipole mechanism are expected, because this means that the luminescent site has an inversion centre. Therefore the magnitude of the crystal field parameters provides an indication of the relative intensity of the absorption spectra and the photoluminescence. The relative magnitude of B^2_0 suggests that Pr^{3+} doped system shows a stronger optical transition than Eu^{3+} doped system.

The crystal field parameters B^k_q also can give an indication of the local symmetry of the dopant ion. From table 3 it is noted that some parameters are zero at both temperatures, indicating that the symmetry of the substitution site is higher. The non-zero values of B^k_q are an indication that a site symmetry involving a D_{2h} element is the most probable one [23]. In $SrAl_{12}O_{19}$, the incorporation of dopant into the lattice does not cause a large deformation that contributes to the loss of local symmetry. This is due to there being relatively large space at the strontium site in $SrAl_{12}O_{19}$ compared with other aluminates. In $SrAl_{12}O_{19}$ the polyhedral volume of the europium and first neighbour ligand ions is 50.54 $Å^3$ [8]. On the other hand, in the $BaAl_2O_4$ lattice, the typical polyhedral volume of europium and first neighbour ligand ions is 40.72 $Å^3$. The

incorporation of europium into the $BaAl_2O_4$ lattice, for example, causes a large deformation resulting in a low symmetry [24].

In table 4 the comparison of the predicted and experimental transition energy of Pr^{3+} in the $SrAl_{12}O_{19}$ matrix are shown, assuming that the substitution is at the Sr^{2+} site accompanied by lattice distortion. It can be seen that the differences between the predicted and the experimental [22] transition energies are small. In addition, the model also provided the right number of states per transition energy, since some of these are hard to identify experimentally.

A better comparison between of the predicted and experimental results was the calculated energy average of each transition. It can be seen from table 5 that the difference between the predicted energy average and experimental is small for all transitions. The same analysis is done for the Eu^{3+} doped system. In table 6 is shown the comparison of the predicted and experimental transition energy for any transition of Eu^{3+} in $SrAl_{12}O_{19}$ structure. In this case, is not possible to compare all transitions due the difficulty of obtaining all transitions in experimental measurement.

4. Conclusion

This paper has presented a computational study of defect and optical properties in $SrAl_{12}O_{19}$. The results were obtained through a combination of three different and complementary techniques: defect calculations through the modelling techniques, crystal field calculation via the simple overlap model and transition energy calculations. The results showed that the Pr preferred to be incorporated at Sr^{2+} sites, with charge compensation by anti-site and Eu^{3+} ion is preferred to be incorporated at the Al^{3+} site. Crystal field parameters have been calculated and the results discussed in terms of optical properties of the doped systems. The transition energy of the Pr^{3+} and Eu^{3+} ions have been calculated and transition energy of Eu^{3+}. B^k_q values indicate that the site symmetry is D_{2h}. The comparison of the predicted transition to the experimental ones gave good agreement in all transition in both rare earths.

Acknowledgments

The authors are grateful to CNPq. CAPES and FINEP for financial support.

References

[1] F. Clabau, X. Rocquefelte, S. Jobic, S. Deniard, M.-H. Whangbo, A. L. Garcia and T. Mercier, Chem. Mater. **17**, 3904 (2005).

[2] L. Yuanhua, Z. Tang, Z. Zhang, Materials Letters **51**, 14 (2001).

[3] C. Chang, D. Mao, J. Shen, C. Feng, J. Alloys Compd. **348**, 224 (2003).

[4] R. Zhong, J. Zhang, X. Zhang, S. Lu, X.-J. Wang, J. Lumin **199**, 327 (2006).

[5] S. Shionoya, W.M. Yen (Eds.), Phosphor Handbook, Chemical. Rubber Company Press, London, 1995, chapter 10.

[6] L. D. Merkle, B. Zandi, R. Moncorge, Y. Guyot, H. R. Verdun and B. McIntosh, J. Appl. Phys. **79**, 1849 (1996).

[7] T. Katsumata. Y. Kohno. H. Kubo. S. Komuro. and T. Morikawa. Review of Scientific Instruments **76**. 084901 (2005)

[8] A. J. Lindop, D. W. Goodwin, Acta Crystallographica **28**, 2625 (1972).

[9] J.D. Gale, J. Chem. Soc.. Faraday Trans. **93**, 629 (1997)

[10] M. V. dos S. Rezende, R. M. Araújo, M. E. G. Valerio and R. A. Jackson, J. Physics: Conference Series **249**, 012042 (2010).

[11] R. M. Araujo, K. Lengyel, R. A. Jackson, L. Kovács, M. E. G. Valerio, J. Phys.: Condens. Matter. **19.** 046211 (2007).

[12] N.F. Mott, M.J. Littleton, Trans. Faraday Soc. **34**. 485 (1938).

[13] O.L. Malta, Chem. Phys. Lett. **88**. 353 (1982).

[14] B.R. Judd, Phys. Rev. **127**. 750 (1962).

[15] G.S. Ofelt, J. Chem. Phys. **37**. 511 (1962).

[16] A.J. Freeman, J.P. Desclaux, J. Magn. Magn. Mater. **12**. 11 (1979).

[17] B.R. Judd, Phys. Rev. **141**. 4 (1966).

[18] H.H. Marvin: Phys. Rev. **71**, 102 (1947)

[19] W.T. Carnall, G.L. Goodman, K. Rajnak, R.S. Rana, J. Chem. Phys. **90**.3443 (1989).

[20] G.K. Liu. at http://chmwls.chm.anl.gov/downloads/spectra/index.html

[21] F.A. Kroger, H.J. Vink, J. Chem. Phys. **22**, 250 (1954).

[22] B. Zandi, L. D. Merkle, J. B. Gruber, D. E. Wortman and C. A. Morrison, J. Appl. Phys. **81** (3),1047 (1997).

[23] K. A. Gschneidner, Jr. and L. Eyring, Handbook on the Physics and Chemistry of Rare Earths, vol. 23 (1996)

[24] M.V. dos, S. Rezende, P.J.R. Montes, M.E.G. Valerio, R.A. Jackson, Opt. Mater. **34**, 1434(2012).

[25] A. M. Srivastavaa, W. W. Beersb, J. Lumin. **71**, 285 (1997).

[26] L. Bo, S. Chao-Shu, Q. Ze-Ming, T. Ye, Chin. Phys. Lett. **22**, 2677 (2005).
[27] Z. Nie, J. Zhang, X. Zhang, X. Ren, W. Di, G. Zhang, D. Zhang and X.-J. Wang, J. Phys.: Condens. Matter **19**, 076204 (2007).
[28] S. Huang, L. Lu, W. Jia, X.-J. Wang, W. M. Tem, A. M. Srivastava, A. A. Setlur, Chem. Phys. Lett. **348**, 11 (2001).
[29] P. A. Rodnyi, P. Dorenbos, G. B. Stryganyuk, A. S. Voloshinovskii, A. S. Potapov and C. W. E. van Eijk, J. Phys.: Condens. Matter **15**, 719 (2003).
[30] V. Singh, J.-J. Zhu and V. Natarajan, phys. stat. sol. **203**, 2058 (2006).
[31] A. D. Deshmukh, S. J. Dhoble, A. Kumar, D. R. Peshwe, S. V. Godbole and M. K. Bhide, Indian J. Pure Appl. Phys. **47**, 444 (2009).

Table 1 – Fractional coordinates of the strontium ion in $SrAl_{12}O_{19}$.

	Fractional coordinates		
Strontium	x	y	z
$Sr^{(i)}$	2/3	1/3	1/4
$Sr^{(ii)}$	5/3	1/3	1/4
$Sr^{(iii)}$	8/3	1/3	1/4
$Sr^{(iv)}$	2/3	4/3	1/4
$Sr^{(v)}$	5/3	4/3	1/4
$Sr^{(vi)}$	2/3	7/3	1/4
Interstitial position	1/3	1/6	1/8

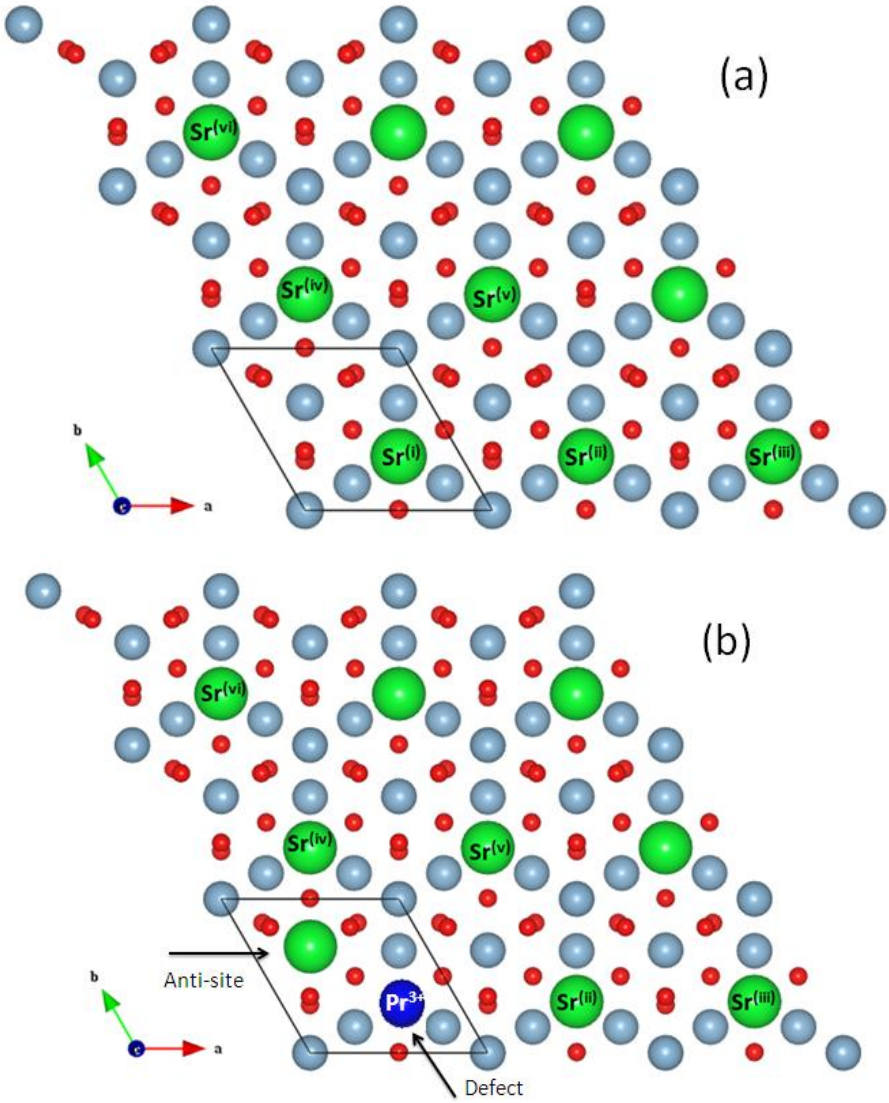

Figure 1 – (a) Positions of strontium ions cited in table 1 (b)Substitution of Pr^{3+} ion at Sr^{2+} sites with charge compensation by anti-site in $SrAl_{12}O_{19}$.

Table 2 – Defect formation energies and solution energy per dopant for Pr and Eu ions at 0 K and 293 K (all energies in eV).

	Formation energy				**Solution energy**			
	Pr		**Eu**		**Pr**		**Eu**	
	0K	**293K**	**0K**	**293K**	**0K**	**293K**	**0K**	**293K**
M_{Al1}	19.60	18.78	17.99	17.21	5.51	4.79	2.70	4.54
M_{Al2}	14.28	13.40	13.12	12.27	0.19	-0.59	0.65	-0.40
M_{Al3}	14.13	13.33	12.98	12.21	0.03	-0.66	**0.24**	**-0.46**
M_{Al4}	18.70	17.92	17.20	16.44	4.61	3.93	2.46	3.77
M_{Al5}	15.34	14.37	14.09	13.16	1.25	0.38	1.36	0.49
$M_{Sr^{(i)}} - Sr_{Al1}^{(i)}$	18.89	18.12	18.23	17.48	4.80	4.13	5.41	4.81
$M_{Sr^{(i)}} - Sr_{Al2}^{(i)}$	14.70	13.82	14.12	13.25	0.61	-0.17	1.30	0.58
$M_{Sr^{(i)}} - Sr_{Al3}^{(i)}$	13.94	13.08	13.31	12.47	**-0.16**	**-0.91**	0.49	-0.20
$M_{Sr^{(i)}} - Sr_{Al4}^{(i)}$	18.38	17.52	17.74	16.90	4.29	3.53	4.92	4.23
$M_{Sr^{(i)}} - Sr_{Al5}^{(i)}$	16.17	15.28	15.54	14.65	2.08	1.29	2.72	1.98
$M_{Sr^{(i)}} - M_{Sr^{(ii)}} - V_{Sr^{(iii)}}$	-23.77	-27.05	-25.06	-28.21	1.49	-0.13	2.12	0.54
$M_{Sr^{(ii)}} - M_{Sr^{(iv)}} - V_{Sr^{(i)}}$	-23.95	-24.56	-25.25	-25.82	1.40	0.70	2.02	1.74
$M_{Sr^{(i)}} - M_{Sr^{(vi)}} - V_{Sr^{(vi)}}$	-23.77	-26.02	-25.06	-27.22	1.49	0.21	2.12	1.04
$M_{Sr^{(i)}} - M_{Sr^{(ii)}} - O_i$	-59.88	-59.17	-59.96	-60.88	0.65	0.94	1.88	1.41
$M_{Sr^{(i)}} - M_{Sr^{(vi)}} - O_i$	-55.85	-59.44	-57.51	-61.85	2.66	0.80	3.11	0.92
$M_{Sr^{(i)}} - M_{Sr^{(v)}} - O_i$	-58.23	-60.43	-58.33	-60.59	1.47	0.31	2.70	1.55
$M_{Sr^{(i)}} - M_{Sr^{(ii)}} - M_{Sr^{(iii)}} - V_{Al1}$	-10.42	-11.05	-12.35	-12.90	0.75	0.54	5.49	1.24
$M_{Sr^{(i)}} - M_{Sr^{(ii)}} - M_{Sr^{(iii)}} - V_{Al2}$	-11.25	-12.15	-13.33	-14.18	0.47	0.17	1.05	0.81
$M_{Sr^{(i)}} - M_{Sr^{(ii)}} - M_{Sr^{(iii)}} - V_{Al3}$	-10.86	-12.68	-12.78	-14.38	0.60	-0.01	1.23	0.75
$M_{Sr^{(i)}} - M_{Sr^{(ii)}} - M_{Sr^{(iii)}} - V_{Al4}$	-10.45	-11.34	-12.36	-13.21	0.73	0.44	1.37	1.14
$M_{Sr^{(i)}} - M_{Sr^{(ii)}} - M_{Sr^{(iii)}} - V_{Al5}$	-9.05	-8.28	-10.93	-11.71	1.20	1.46	1.85	1.64
$M_{Sr^{(i)}} - M_{Sr^{(vi)}} - M_{Sr^{(v)}} - V_{Al1}$	-10.10	-11.40	-12.03	-13.21	0.85	0.42	1.48	1.14
$M_{Sr^{(i)}} - M_{Sr^{(vi)}} - M_{Sr^{(v)}} - V_{Al2}$	-10.88	-12.54	-12.98	-14.47	0.59	0.04	1.16	0.72
$M_{Sr^{(i)}} - M_{Sr^{(vi)}} - M_{Sr^{(v)}} - V_{Al3}$	-10.81	-12.19	-12.73	-13.96	0.62	0.16	1.25	0.89
$M_{Sr^{(i)}} - M_{Sr^{(vi)}} - M_{Sr^{(v)}} - V_{Al4}$	-10.28	-11.20	-12.05	-12.93	0.79	0.49	1.47	1.23
$M_{Sr^{(i)}} - M_{Sr^{(vi)}} - M_{Sr^{(v)}} - V_{Al5}$	-7.55	-9.72	-9.59	-11.52	1.70	0.98	2.29	1.70
$M_{Sr^{(i)}} - M_{Sr^{(vi)}} - M_{Sr^{(vi)}} - V_{Al1}$	-10.43	-11.01	-12.35	-12.86	0.74	0.55	1.37	1.25
$M_{Sr^{(i)}} - M_{Sr^{(vi)}} - M_{Sr^{(vi)}} - V_{Al2}$	-11.38	-12.22	-13.46	-14.25	0.43	0.15	1.00	0.79
$M_{Sr^{(i)}} - M_{Sr^{(vi)}} - M_{Sr^{(vi)}} - V_{Al3}$	-10.86	-12.84	-12.79	-14.52	0.60	-0.06	1.23	0.70
$M_{Sr^{(i)}} - M_{Sr^{(vi)}} - M_{Sr^{(vi)}} - V_{Al4}$	-10.50	-11.36	-12.42	-13.38	0.72	0.43	1.35	1.08
$M_{Sr^{(i)}} - M_{Sr^{(vi)}} - M_{Sr^{(vi)}} - V_{Al5}$	-9.05	-9.95	-9.37	-11.74	1.20	0.90	2.37	1.63

Table 3– B^k_q values (cm^{-1}) for the relaxed lattice at 293 K in strontium sites.

	Pr			Eu		
B^k_q	**No-relax.**	**Relax.**	**Fen. [22]**	**No-relax.**	**Relax.**	**Fen. [22]**
B^2_0	189.60	332.55	-155	144.12	278.99	-147
B^2_1	0.00	0.00	-	0.00	0.00	-
B^2_2	2.53	-17.17	-	1.93	-20.36	-
B^4_0	449.88	481.71	763	267.12	286.10	571
B^4_1	0.00	0.00	-	0.00	0.00	-
B^4_2	4.69	-14.38	-	2.78	-10.81	-
B^4_3	0.00	0.00	-	0.00	0.00	-
B^4_4	-0.73	-4.86	-	-0.43	-3.61	-
B^6_0	-1332.50	-1693.35	-1792	-640.87	-844.11	-1195
B^6_1	0.00	0.00	-	0.00	0.00	-
B^6_2	2.94	-28.29	-	1.41	-17.74	-
B^6_3	0.00	0.00	-	0.00	0.00	-
B^6_4	-0.50	-22.05	-	-0.24	-12.08	-
B^6_5	0.00	0.00	-	0.00	0.00	-
B^6_6	756.42	930.80	-1419	363.80	459.85	-946

Table 4 – Comparison of the predicted and experimental energy (nm) transition of Pr^{3+} in the $SrAl_{12}O_{19}$ matrix at 293K.

Term	Cal.	Theory	Exp.[22]	Term	Cal.	Theory	Exp.[22]
	213.0	-	-		249.8	249.7	-
	213.0	213.3	-		249.9	250.0	250.0
	213.7	213.6	-		250.0	-	-
	213.7	-	-		250.0	-	-
$^1S_0 \rightarrow {}^4H_4$	213.9	213.9	-	$^1S_0 \rightarrow {}^3F_4$	250.1	250.4	250.4
	214.0	214.0	214.0		250.1	250.6	-
	214.0	214.1	-		250.5	251.2	251.1
	214.7	-	-		250.7		-
	215.2	215.7	-		250.7	251.3	-
	223.1	-	-		268.4	269.0	-
	223.1	-	-		268.5	-	268.8
	223.6	223.8	-		269.9	269.5	-
	223.7	223.9	-		270.0	270.0	270.0
	223.7	224.0	224.0	$^1S_0 \rightarrow {}^1G_4$	270.3	-	-
$^1S_0 \rightarrow {}^4H_5$	224.1	-	-		270.4	270.7	-
	224.1	224.0	224.1		271.0	272.9	-
	224.5	-	-		272.9	-	-
	224.6	224.2	224.3		273.0	273.7	273.8
	224.7	225.3	225.3		333.4	331.9	-
	224.7	225.5	-		333.5	332.9	332.9
	233.8	-	-	$^1S_0 \rightarrow {}^1D_2$	333.7	-	-
	233.8	234.1	234.1		334.7	334.2	334.2
	234.0	234.2	-		334.8	-	-
	234.5	234.5	234.5	$^1S_0 \rightarrow {}^3P_0$	383.8	382.6	382.6
	234.6	234.6	-		389.5	390.7	-
$^1S_0 \rightarrow {}^4H_6$	235.5	235.4	-	$^1S_0 \rightarrow {}^1I_6$	389.6	390.7	390.8
	235.8	235.6	-		392.0	391.2	-
	235.8	-	-		392.2	-	-
	236.1	-	-	$^1S_0 \rightarrow {}^3P_1$	392.2	392.7	392.7
	236.1	-	-		392.5	393.1	393.2
	236.2	236.3	236.4	$^1S_0 \rightarrow {}^1I_6$	392.5	393.7	-

	236.8	236.8	236.9		392.6	-	-
	236.8	237.2	-		393.9	394.3	-
	239.5	239.6	239.8		394.2	394.3	394.3
	239.5	-	-		395.6	294.5	-
$^1S_0 \rightarrow {}^3F_2$	239.6	-	-		395.8	-	-
	239.6	240.1	240.0		395.9	-	-
	239.6	240.2	240.0		396.2	397.7	397.8
	246.8	246.5	-		396.7	-	-
	247.3	247.0	247.0		396.7	398.4	-
	247.3	-	-		411.9	410.7	410.5
$^1S_0 \rightarrow {}^3F_3$	247.4	247.4	-		412.1	410.7	-
	248.1	247.9	-	$^1S_0 \rightarrow {}^3P_2$	412.2	-	-
	248.2	247.1	-		414.2	412.4	-
	248.2	-			414.2	-	412.6

Table 5 – Comparison between average calculated energy (nm) and experimental and other theory transition to Pr^{3+}:$SrAl_{12}O_{19}$.

Term	Average calculated	Experimental and other theory transition
$^1S_0 \rightarrow {}^4H_4$	213.9	220[25] 215[27] 214.0(t)[22] 214.1(e)[22]
$^1S_0 \rightarrow {}^4H_5$	224.0	224.4(t)[22] 224.4(e)[22]
$^1S_0 \rightarrow {}^4H_6$	235.4	235.5(t)[22] 235.4(e)[22]
$^1S_0 \rightarrow {}^3F_2$	239.6	239.9(t)[22] 239.9(e)[22]
$^1S_0 \rightarrow {}^3F_3$	247.6	247.0(t)[22] 247.4(e)[22]
$^1S_0 \rightarrow {}^3F_4$	250.2	253.4[29] 254[27] 253[28] 250.5(t)[22] 250.5(e)[22]
$^1S_0 \rightarrow {}^1G_4$	270.5	273.6[28] 276.6[25] 275[27] 273.6[28] 270.9(t)[22] 271.0(e)[22]
$^1S_0 \rightarrow {}^1D_2$	334.0	342[25] 343.4[28] 333.5(t)[22] 333.0(e)[22]
$^1S_0 \rightarrow {}^3P_0$	383.8	382.6(t)[22] 382.6(e)[22]
$^1S_0 \rightarrow {}^1I_6$	390.8	402[29] 404[25]

		403[26] 402(e)[27] 406.3(e)[28] 390.8(t)[22] 390.9(e)[22]
$^1S_0 \rightarrow {}^3P_1$	392.4	392.9(t)[22] 392.9(e)[22]
$^1S_0 \rightarrow {}^1I_6$	395.0	396.0(t)[22] 395.5(e)[22]
$^1S_0 \rightarrow {}^3P_2$	412.9	411.6(t)[22] 411.3(e)[22]

Table 6 – Comparison between average calculated energy (nm) and experimental and other theory transition to Eu^{3+}:$SrAl_{12}O_{19}$.

Term	Cal.	Average Cal.	Experimental
$^5D_0 \rightarrow {}^7F_0$	563.8	563.8	-
$^5D_0 \rightarrow {}^7F_1$	578.8 579.4 581.8	580.0	592[30]; 578[31]
$^5D_0 \rightarrow {}^7F_2$	602.2 602.2 603.8 604.6 604.7	603.0	616[30]